Characteristics and Trends of the Campbell Plateau Meander in the Southern Ocean: 1993-2020

Xinlong Liu[1,2,3*], Amelie Meyer[1,2], and Christopher C. Chapman[4,5]

[1]Institute for Marine and Antarctic Studies, University of Tasmania, Hobart, TAS, Australia.
[2]Australian Research Council Centre of Excellence for Climate Extremes, University of Tasmania, Hobart, TAS, Australia.
[3]Overseas Learning Centre, University of Tasmania, Qingdao, Shandong, China.
[4]CSIRO (Commonwealth Scientific and Industrial Research Organisation) Environment, Earth Systems Science Program, Hobart, TAS, Australia.
[5]Centre for Southern Hemisphere Oceans Research (CSHOR), Hobart, TAS, Australia.

Key Points:

- The position of the Campbell Plateau meander has remained stable for the past 30 years, apart from a section downstream shifting northward.
- The amplitude of the Campbell Plateau meander has been decreasing (flatter) upstream from the Plateau and increasing downstream.
- The Campbell Plateau meander has been widening and accelerating over the 1993 to 2020 period, especially downstream from the Plateau.

*Current address: Institute for Marine and Antarctic Studies, 20 Castray Esplanade, Battery Point, TAS, Australia 7004

Corresponding author: Xinlong Liu, `xinlong.liu@utas.edu.au`

Abstract

Meanders are significant features of the Antarctic Circumpolar Current in the Southern Ocean and sites of enhanced upwelling, cross-frontal tracer fluxes, and exchanges between the surface and deep ocean. They usually overlap the locations of fronts and are linked to topographic features. While much is known about Southern Ocean fronts and how they are changing, the response of meanders to climate change is largely unexplored. In this study, we investigate the Campbell Plateau meander south of New Zealand. We apply a local gradient maxima method to satellite altimetry data to identify the position of the meander and estimate its width, geostrophic current speed and associated trends over the 1993-2020 period. We find that the position of the meander has been relatively fixed, except for the section downstream from the Plateau, which has shifted northward by about 0.4° latitude per decade. The meander has become flatter at the Plateau's western edge, but steeper at the eastern edge of the Plateau. Overall, the meander has been widening by 2 km per decade and accelerating by 0.01 m s^{-1} per decade, particularly downstream from the Plateau. These findings are consistent with other work on standing meanders and observed changes in the Southern Ocean. While we cannot attribute the observed trends of the Campbell Plateau meander to one particular forcing mechanism, we discuss several hypotheses in the context of existing literature. Whether these trends are similar for other Southern Ocean meanders and their implications remains to be verified.

Plain Language Summary

In the Southern Ocean, meanders are parts of the Antarctic Circumpolar Current that deviate from the usual west-to-east flow by having a substantial north-south component, resulting in a wave-like appearance. Standing meanders are meanders that are stationary and do not move much over months and years. They are a special feature of the Antarctic Circumpolar Current and are fundamental for exchanges between the surface and deep ocean. While changes in the Antarctic Circumpolar Current have been well studied, especially in the context of climate change, very little is known about how Southern Ocean meanders are changing. This study focuses on the Campbell Plateau meander south of New Zealand in the Southern Ocean. Using ocean sea surface height data from satellites, we analyse the monthly position of this meander, estimate its monthly width and speed, and quantify how these characteristics have changed over the 1993-2020 period. Upstream from the Campbell Plateau, the meander has undergone almost no changes in its position, width or speed. However, downstream from the Plateau, the meander has shifted northward, widened and accelerated. These trends are consistent with other observations in the Southern Ocean and we discuss potential mechanisms to explain them.

1 Introduction

The Southern Ocean is crucial in the context of global climate by being a major sink of anthropogenic heat and carbon dioxide (Rintoul & Naveira Garabato, 2013; Frölicher et al., 2015; Bindoff et al., 2019) through the upwelling of deep waters and their subsequent downwelling, which produces a large proportion of global deep waters (Toggweiler & Samuels, 1995; Lumpkin & Speer, 2007; J. Marshall & Speer, 2012; Morrison et al., 2015). The Southern Ocean has absorbed about 40% of global oceanic carbon dioxide over the last two centuries (Sabine et al., 2004; Mikaloff Fletcher et al., 2006; Sallée et al., 2012). In the Southern Ocean, the predominant circulation feature is the deep-reaching Antarctic Circumpolar Current, which manifests as the southward shoaling of vigorously tilted isopycnals (Rintoul & Naveira Garabato, 2013) and carries approximately 170 Sv (Sverdrup; 1 Sv = 10^6 m^3 s^{-1}) of water eastward (Donohue et al., 2016). Primarily driven by the strong mid-latitude westerly winds and buoyancy forcing, the Antarctic Circumpolar Current links the Atlantic, Indian, and Pacific Oceans, conveying climate signals through the transport of heat, momentum, and other tracers (Sabine et al., 2004; Sarmiento et al., 2004; Olbers et al., 2004; Sallée et al., 2012; Rintoul & Naveira Garabato, 2013).

In the Southern Ocean, the transition from warmer subtropical waters to colder Antarctic waters as one travels south does not occur smoothly but is instead concentrated into a series of sharp transition zones (Deacon, 1937), called 'fronts', which are generally east-west aligned (Deacon, 1937; Chapman et al., 2020; Thomas et al., 2021). Fronts delimit the borders of separate water masses that each have their own unique environmental characteristics (Orsi et al., 1995) and tend to correspond to sites of the Antarctic Circumpolar Current's narrow, high-velocity currents known as 'jets' (Sokolov & Rintoul, 2002, 2007b). These fronts suppress the meridional exchange of heat and tracers in the Southern Ocean (Naveira Garabato et al., 2011; Thompson & Sallée, 2012; Chapman & Sallée, 2017).

In some regions of the Southern Ocean, these fronts have a non-zonal orientation (Hughes, 2005; Sokolov & Rintoul, 2007a). Such 'meanders' are generated by the interactions between the Antarctic Circumpolar Current and large topographic features (Thompson, 2010; Thompson & Sallée, 2012; Dove et al., 2021, 2022) such as the Campbell Plateau and the Kerguelen Plateau (e.g., Roach et al. (2016); Klocker (2018)). Standing meanders are meanders that have little to no temporal variability: they follow the same path over time. Several standing meanders such as the Campbell Plateau standing meander and the Agulhas-Kerguelen standing meander (e.g., Meyer et al. (2023)) are found along the Antarctic Circumpolar Current. The Southern Ocean standing meander regions are recognised as dynamical hotspots, where upwelling (Viglione & Thompson, 2016; Tamsitt et al., 2017; Brady et al., 2021), subduction (Llort et al., 2018; Bachman et al., 2017; Dove et al., 2021), cross-frontal exchanges (Langlais et al., 2011; Thompson & Sallée, 2012), vertical momentum transport (Thompson & Naveira Garabato, 2014), and eddy energy (Gille & Kelly, 1996; Witter & Chelton, 1998; Lu & Speer, 2010; Chapman et al., 2015; Rosso et al., 2015; Foppert et al., 2017) are enhanced. Standing meanders can greatly impact horizontal current transport with strong meridional deviations from the zonal flow of up to 5° latitude (Nardelli, 2013; Phillips & Bindoff, 2014; Thompson & Naveira Garabato, 2014). Thompson and Naveira Garabato (2014) also show that the meanders 'flex' under wind forcing, and this response propagates vertically through the water column. Compared with quieter downstream regions, Southern Ocean standing meanders regions stand out with larger lateral buoyancy gradients in mixed layer, increased variability in mixed layer depth, and show signs of stronger ocean mixing (Thompson & Naveira Garabato, 2014; Langlais et al., 2017)

While studies have been undertaken to assess the response of the Antarctic Circumpolar Current fronts to climate change, less work has focused on meanders and their trends. A majority of meander studies have looked at dynamic mechanisms, energy transport, and their role in the Southern Ocean system (e.g., Thompson and Sallée (2012); Chapman et al. (2015); Barthel et al. (2017); Youngs et al. (2017); Barthel et al. (2022); Meijer et al. (2022); X. Zhang et al. (2022); Cyriac et al. (2023)). Although a few studies have investigated long-term changes and trends of meanders whether, in response to climate change, natural variability and changes in dynamics, such as Thompson and Naveira Garabato (2014) and Meyer et al. (2023), further research is needed to fully understand the trends of meanders over time. By modelling several Southern Ocean standing meanders, Thompson and Naveira Garabato (2014) report the response of meanders to increased wind forcing which includes steeper isopycnals, increased curvature, and changing wavelength and amplitude of the meanders. An observational study of the Agulhas-Kerguelen standing meander in the southwest Indian Ocean has also identified trends in the curvature of the meander, its width and speed over the past 30 years (Meyer et al., 2023).

Considering the importance of meanders in the Southern Ocean, it is key that we better understand how they are changing and what the impacts of these changes might be on the climate system. In this study, we apply a "local" front detection method on satellite altimetry data to identify and characterise the trends of the Campbell Plateau meander in the Southern Ocean over the 1993-2020 period. The Campbell Plateau is located in the southwestern Pacific sector of the Southern Ocean and most areas of the Plateau are shallower than 1000 m depth (Neil et al., 2004; Forcén-Vázquez et al., 2021). It extends about 1100 km southeast of the South Island, New Zealand. The Plateau largely constrains the eastward flow of the Antarctic Circumpolar Current (Gordon, 1972; Orsi et al., 1995), which leads to a significant northward deviation of the Antarctic Circumpolar Current along its eastern boundary (Heath, 1981; Carter & Wilkin, 1999; Morris et al., 2001). The Antarctic Circumpolar Current front forming the Campbell Plateau meander follows the southern edge of the Plateau. We find that, overall, the Campbell Plateau meander has been relatively spatially stable except for its downstream section which has moved northward. The meander has been significantly widening and accelerating over the 1993-2020 period. For the remaining sections of this paper, Section 2 describes the data and the meander analysis methods. Section 3 shows the characteristics and identified trends of the meander. In Section 4, we discuss the implications, and, finally, we summarise the key findings of this study in Section 5.

2 Data and Methods

2.1 Satellite Altimetry Data

In this study, we use the AVISO absolute dynamic topography and surface geostrophic current speeds products from multi-mission satellite altimetry (CMEMS, 2019) spanning over the 1993-2020 period to identify and characterise the Campbell Plateau meander.

2.2 Meander Position Identification

The meander position identification methodology used in this study belongs to the broader family of "local gradient maxima" methods (Chapman, 2017; Chapman et al., 2020). Chapman (2017) applied this methodology to fronts in the Southern Ocean. The method was then modified by Meyer et al. (2023) for the Agulhas-Kerguelen standing meander and further adjusted in this study for the Campbell Plateau meander. Generally speaking, there are two kinds of definitions for Southern Ocean fronts and thus meanders: local definitions and global definitions (Chapman et al., 2020). In this study, we focus on local definitions. Local definitions use properties found in the local vicinity of a geographical position to evaluate if a front exists (Chapman et al., 2020). The 'gradient thresholding' method is perhaps used most frequently. In this method, a front or meander is identified when the gradient of a quantity (e.g., sea surface temperature: Moore et al. (1999); Dong et al. (2006); Freeman et al. (2016) or sea surface height: Hughes and Ash (2001); Chapman (2014, 2017)) is larger than a predetermined threshold value.

In this study, we choose to employ the local gradient method as sea surface height contours used in the global method are impacted on longer time scales by the large-scale steric height tendency that is linked to the Southern Ocean warming (Gille, 2014). As pointed out by Sokolov and Rintoul (2009), it is challenging to identify in long-term position trends of sea surface height contours what is driven by frontal displacement and what is driven by sea level increases (Gille, 2014). Although some studies have explored frontal position changes using satellite sea surface temperature data (e.g., Moore et al. (1997, 1999); Dong et al. (2006)), we choose absolute dynamic topography because it captures both surface and subsurface ocean processes (McDougall & Klocker, 2010), while sea surface temperature represents only ocean surface conditions. Here, we do not consider the Campbell Plateau meander's vertical structure but only surface properties obtained from the altimetric product. Since the Antarctic Circumpolar Current is approximately equivalent barotropic (Killworth, 1992), particularly when averaged over several eddy time cycles (Phillips & Bindoff, 2014). As such, we assume that the surface signature of the meander is broadly reflective of the current at depth.

W apply three main steps to identify the position of the Campbell Plateau meander:

1. Derive the **gradients** of absolute dynamic topography in the Campbell Plateau region (30°S-70°S and 150°E-210°E; shown in Figure 1 (a) and (b)).
2. Identify **daily position** of the meander. This is defined as areas where the absolute dynamic topography gradient exceeds a relative threshold. This definition is then applied to every daily snapshot of the absolute dynamic topography gradient maps over the 1993-2020 period to mark the meander signals. Selecting the appropriate relative threshold value requires striking a balance between identifying enough meander signals without including too many non-meander features such as eddies. We choose 25% of the maximum absolute dynamic topography gradient as the relative threshold based on sensitivity tests (see Figure B.1 in Appendix B.1 of X. Liu (2022) for details).
3. Obtain the **time-averaged positions** of the meander. By summing the total number of times that the meander is identified at each point in the Campbell Plateau region over a certain period of time, we derive the meander frequency (similar to the frontal frequency in Chapman (2017)), which we can use to produce the meander's monthly occurrence maps over a period of several months. We choose a 4-month period as it smooths out the shorter time-scale variability including eddies, and retains the longer-term signals that are of interest (see Figure B.2 in Appendix B.2 of X. Liu (2022) for details).

The final product is the monthly longitude and latitude position of the meander. We zoom into a subsection of our domain (46°S-57°S and 150°E-210°E; Figure 1 (b), blue rectangle), which is the smallest area where we can identify the meander continuously in the Campbell Plateau region, to enable us to ignore frontal signals detected outside the marked meander area. Next, we determine the peak meander frequency at each latitude and longitude in this smaller domain, which identifies the position of the meander (Figure 2 (b) and (c) red star). We note that the monthly meander position sometimes has 'jumps' and 'spikes' (Figure 2 (a), blue line). These 'jumps' are usually due to eddies freshly detached from the meander that have a strong gradient in absolute dynamic topography (see Figure B.3 in Appendix B.3 of X. Liu (2022) for an example).

2.3 Meander Characteristics

We estimate the meander width by using the meander frequency: for each longitude, the width of the meander is taken to be the sum of the meridional distances between the latitude of the meander frequency peak and latitude where the frequency is zero to the north and south (northern and southern boundaries) (Figure 2, blue line in (b) and blue arrow in (c)). We also identify the monthly position of four key standing peaks and four troughs of the meander and estimate the monthly amplitude in two regions (Table 1; Figure 3). We define the peaks as the southernmost points (farthest distance from the equator) and troughs as the northernmost (in closest proximity to the equator) points of the meander's trajectory (Newton, 1959; Meijer et al., 2022) for each month, within the manually-defined longitude ranges (Table 1). These peaks and troughs are consistently identifiable over the 1993-2020 period and are labelled Pk 1 to Pk 4 and Tr 1 to Tr 4 from west to east (Figure 3). The amplitude of the meander at two sets of peaks and troughs is then estimated as half of the meridional distance (in degrees latitude) between these adjacent peaks and troughs. While identifying the positions of the peaks and troughs is automated, quality control involves manual checks. We also calculate the monthly geostrophic current speed over the 4-month sum period using the daily zonal (U_{geos}) and meridional (V_{geos}) geostrophic velocities.

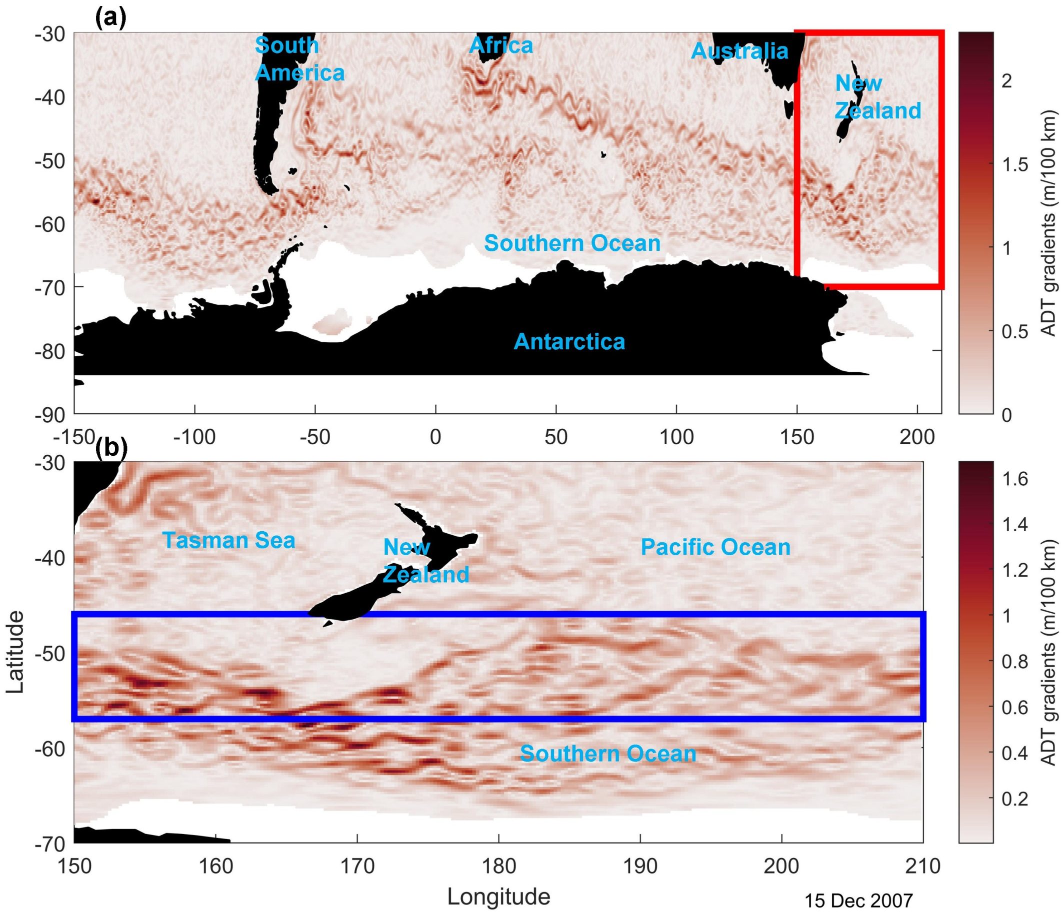

Figure 1. Snapshot of the absolute dynamic topography (ADT) gradients in m/100 km on 15 December 2007 in (a) the Southern Ocean and (b) the Campbell Plateau region. The red rectangle in (a) represents the Campbell Plateau region shown in (b), which is the study region. The blue rectangle in (b) indicates the smaller domain where the meander's latitude and longitude positions are identified. White areas are regions where no satellite altimetry data were available.

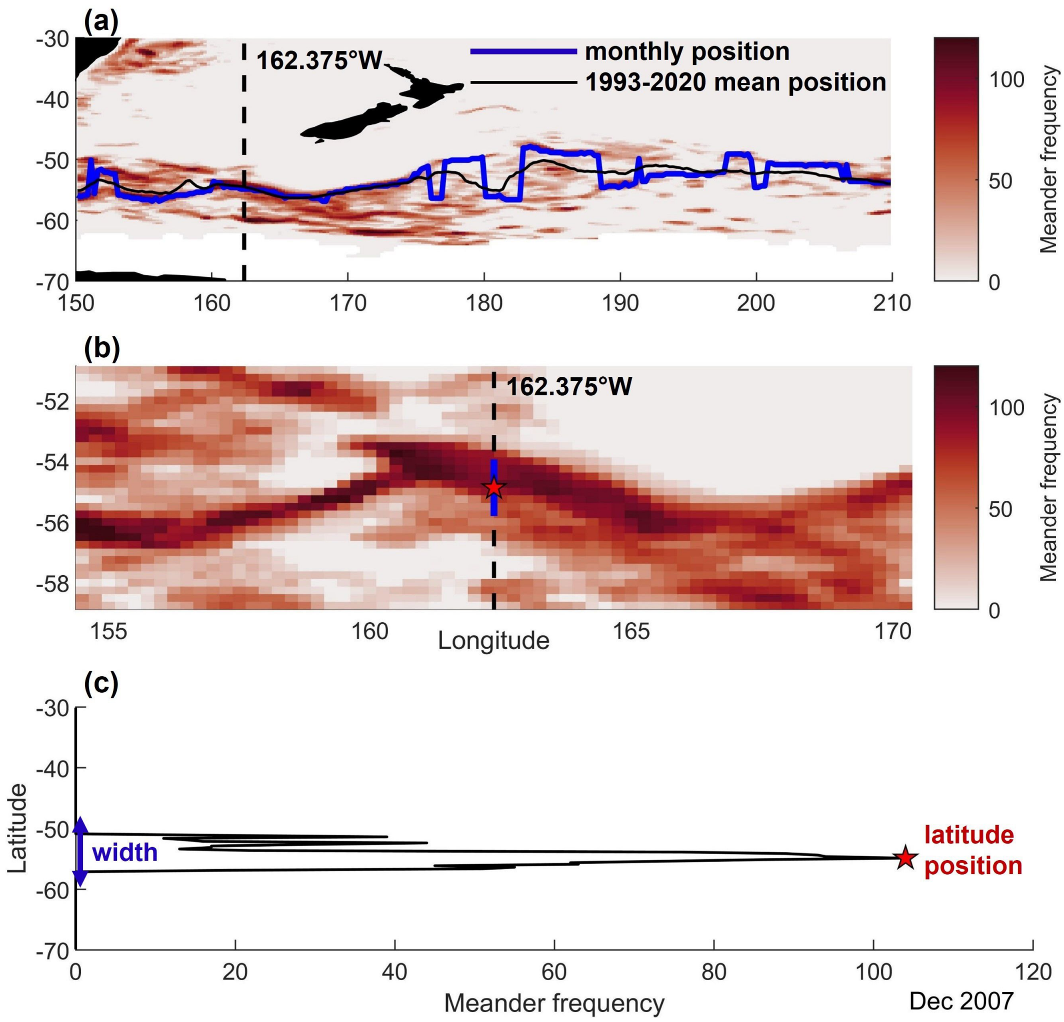

Figure 2. (a) Meander's monthly position (thick blue line) for December 2007 and 1993-2020 meander mean position (thin black line) over the meander frequency occurrence for the 4-month sum period; (b) Meander's width range (vertical solid blue line) together with its latitude position (red star) at 162.375°W over the meander frequency occurrence for the 4-month sum period; (c) Meander frequency transect at 162.375°W with meander latitude position (red star) and width range (blue arrow). White areas in (a) are regions where no satellite altimetry data were available.

Table 1. Longitude ranges of the peaks, troughs, and sections of the Campbell Plateau meander.

	Longitude Ranges
Meander Peaks	
Peak 1	156.6°E-157.1°E
Peak 2	159.1°E-159.6°E
Peak 3	164.9°E-165.9°E
Peak 4	180.2°E-181.4°E
Meander Troughs	
Trough 1	157.9°E-158.6°E
Trough 2	159.9°E-160.9°E
Trough 3	177.1°E-177.6°E
Trough 4	183.9°E-184.9°E
Meander Sections	
Upstream Section	150.0°E-158.4°E
Plateau Section	158.4°E-184.4°E
Downstream Section	184.4°E-210°E
Flat Region	191.6°E-204.9°E

2.4 Statistical Trends

To investigate trends in the position, width and geostrophic current speed of the meander for the 1993-2020 period, we apply a linear regression to the monthly time series. Then, a time-lagged analysis using multiple linear regression ($\hat{y} = b_0 + b_1x_1 + b_2x_2 + ... + b_kx_k$) is applied to all the derived trends to test for statistical significance. Each of the k predictor variables has a coefficient corresponding to the slope in the linear regression. The intercept (or regression constant) is expressed as b_0. These k + 1 coefficients are often recognised as the regression parameters. We also test for autocorrelations in the time series and the associated autocorrelation time scales. In this study, we choose a 3-month lag as it removes part of the seasonal and sub-seasonal variability in the time series that we are not investigating and is adequately short to avoid the potential autocorrelation time scales of the dataset. The sample autocorrelation functions of the monthly trends and their 95% confidence intervals are also estimated using the test of residual analysis with autocorrelation. Detailed figures for these autocorrelation tests are in Appendix A of X. Liu (2022).

3 Results

3.1 Meander Trajectory

By investigating the trajectory of the meander, we identify 4 areas in the Campbell Plateau region where the meander dynamics are distinct: an 'Upstream Section' west of the Campbell Plateau, a 'Plateau Section' south of the Plateau, a 'Downstream Sec-

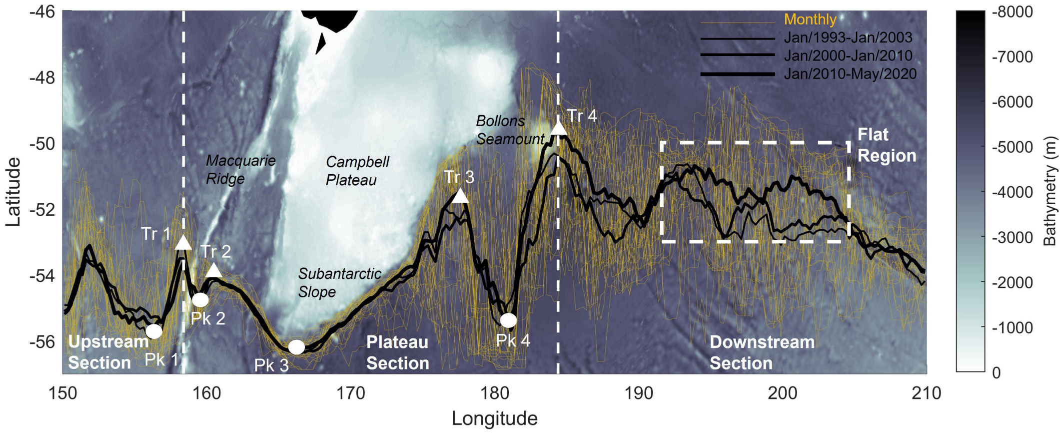

Figure 3. The Campbell Plateau meander's mean positions over three different decades (black lines) and monthly positions at the ten-month interval (yellow lines) between 1993 and 2020. Four peaks (white circles) and four troughs (white triangles) of the meander are marked along the meander's trajectory (Pk 1 to Pk 4 and Tr 1 to Tr 4). Also indicated are the three sections (Upstream, Plateau, and Downstream) of the meander separated by two white vertical dashed lines and the Flat Region (white dashed rectangle) is highlighted.

tion' east of the Plateau, and a 'Flat Region' farther downstream from the Plateau where the shape of the meander is flatter than in other sections (Figure 3; details in Table 1).

The meander enters the study domain from the west at approximately 55°S (Figure 3, Upstream Section). It encounters and is modified by the Macquarie Ridge (Figure 3, Trs 1 and 2; Pks 1 and 2). When the meander encounters the Macquarie Ridge, its long-term mean position flows through a shallower canyon (2000 m depth; at about 52.0°S) rather than the deeper canyon (4000 m depth; at about 53.3°S) (Figure 3, Upstream Section). However, we note that at shorter time scales of about one month, the meander switches between these two canyons (Chapman & Morrow, 2014; Rintoul et al., 2014). Next, the meander continues to flow eastward and is steered by the Campbell Plateau and the Subantarctic Slope, flowing along a boundary between 4000 m and 6000 m deep (Figure 3, Plateau Section). Eventually, the current flows into the Downstream Section, where the interaction between the meander and topography is weaker than upstream, with almost no topographic impact except near the far eastern boundary (Figure 3, Downstream Section). The trajectory in the Downstream Section is relatively flat (less flexed) with fewer wave features, especially in the highlighted 'Flat Region' (Figure 3, Flat Region). We also find that the locations of the peaks and troughs are related to the regional topography with several peaks and troughs associated with local ridges, seamounts and other topographic features (Figure 3).

3.2 Observed Changes in Meander Position

We now investigate the temporal trends of the meridional displacement, width, and geostrophic current speed of the Campbell Plateau meander to understand the long-term changes (if any) of this meander system. We estimate these trends based on both the full-resolution monthly time series and a smoothed rolling-mean time series. The trends for the meridional displacement, width, and geostrophic current speed of this meander are very similar whether from the monthly time series or from the rolling-mean data (not shown) and here, we present the monthly data results.

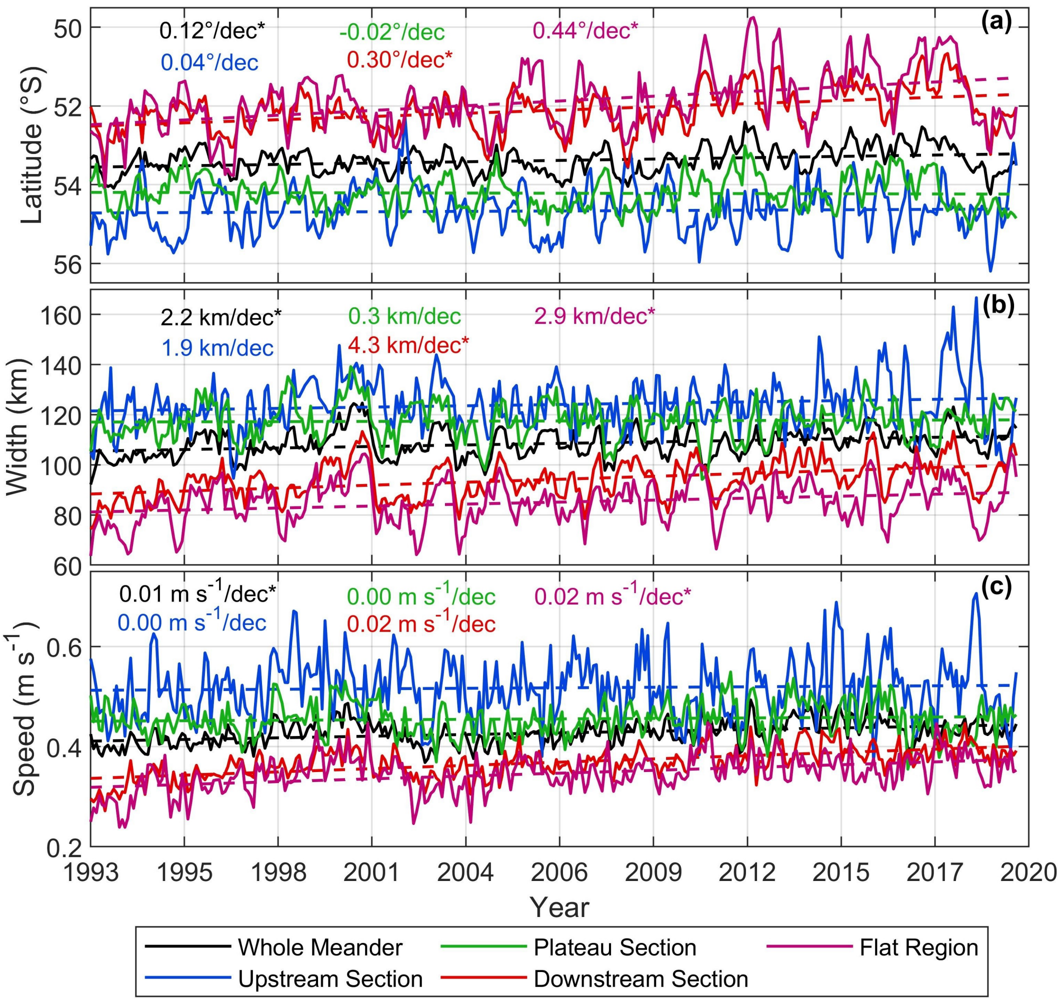

Figure 4. Monthly time series (solid lines) and corresponding linear trends (dashed lines) over the 1993-2020 period of the Campbell Plateau meander's (a) mean latitude position (degrees latitude per decade), (b) width (km per decade), and (c) geostrophic current speed (m s^{-1} per decade). Positive trend values in the mean latitude position, width, and geostrophic current speed represent the northward movement, widening, and accelerating of the meander; while negative trends indicate the southward movement, narrowing, and decelerating of the meander. Statistically significant trends are indicated with '*'.

We find that the mean position of the whole meander has been moving northward by 0.12° latitude per decade from 1993 to 2020 (Figure 4 (a); Table 2). This overall trend hides regional variations in displacement (Figure 4 (a); Table 2). Apart from some small-scale variability, the Upstream and Plateau Sections of the meander are relatively stationary between 1993 and 2020 with small non-significant trends (0.04° and -0.02° latitude per decade, respectively; Figure 3, Upstream and Plateau Sections; Figure 4 (a)). In contrast, the Downstream Section has a significant northward moving trend of 0.30° latitude per decade (R^2=0.324, p=0.000; Figure 4 (a); Table 2). This significant northward trend is even stronger in the Flat Region (0.44° latitude per decade; R^2=0.349, p=0.000; Figure 4 (a); Table 2). This regional analysis indicates that the slight northward trend of the whole meander (0.12° latitude per decade) is dominated by that of the meander downstream from the Plateau and, particularly, in the Flat Region.

Table 2. Linear decadal trends and their associated statistics for the Campbell Plateau meander's meridional displacement (position) in degrees latitude per decade (° lat/dec), width in km per decade (km/dec), and geostrophic current speed (speed) in m s^{-1} per decade (m s^{-1}/dec) based on the monthly data time series over the 1993-2020 period. Statistically significant trends are indicated with *.

	Position (° lat/decade)	*Width (km/decade)*	*Speed (m s^{-1}/decade)*
Whole Meander	+0.12* (R^2=0.264, p=0.000)	+2.20* (R^2=0.213, p=0.000)	+0.01* (R^2=0.120, p=0.000)
Upstream Section	+0.04 (R^2=0.030, p=0.007)	+1.90 (R^2=0.000, p=0.000)	0.00 (R^2=0.010, p=0.450)
Plateau Section	-0.02 (R^2=0.160, p=0.007)	+0.30 (R^2=0.094, p=0.000)	0.00 (R^2=0.020, p=0.000)
Downstream Section	+0.30* (R^2=0.324, p=0.000)	+4.20* (R^2=0.302, p=0.000)	+0.02 (R^2=0.000, p=0.000)
Flat Region	+0.44* (R^2=0.349, p=0.000)	+2.90* (R^2=0.164, p=0.000)	+0.02* (R^2=0.230, p=0.000)

Table 3. Meridional displacement (latitude position) trends of the peaks and troughs of the Campbell Plateau meander in degrees latitude per decade (° lat/dec) based on the monthly data time series over the 1993-2020 period. Positive trend values indicate northward movements while negative trends indicate southward movements of peaks and troughs.

	Trough 1	Trough 2	Trough 3	Trough 4
Position (° lat/dec)	-0.17 (R^2=0.018, p=0.052)	-0.02 (R^2=0.001, p=0.585)	+0.39 (R^2=0.024, p=0.159)	+0.10 (R^2=0.003, p=0.361)
	Peak 1	Peak 2	Peak 3	Peak 4
Position (° lat/dec)	+0.05 (R^2=0.002, p=0.593)	+0.26 (R^2=0.122, p=0.000)	+0.03 (R^2=0.014, P=0.091)	-0.31 (R^2=0.035, p=0.001)

Investigating the meridional displacement trends of individual peaks and troughs of the meander between 1993 and 2020 shows that their migrations are not statistically significant, quite noisy, and of mixed signs (Table 3): some have moved northward (Trough 4 and Peak 2: 0.10° and 0.26° latitude per decade, respectively), some southward (Trough 1: -0.17° latitude per decade), while some are relatively stationary (Trough 2 and Peak 3: -0.02° and 0.03° latitude per decade, respectively). While the changes are not significant, some of these peaks and troughs have shifted meridionally over the 1993-2020 period: Trough 3 shows a non-significant northward trend of 0.39° latitude per decade, and Peak 4 has a southward moving trend of 0.31° latitude per decade.

Based on the meridional displacement trends of the paired peaks and troughs, we derive a time series of the meander amplitude in two places along its trajectory as half of the meridional distance between the selected pair of peaks and troughs and estimate the trends of these two wave amplitudes over the 1993-2020 period. Wave 1, composed of Trough 1 and Peak 2, is upstream from the Campbell Plateau, while Wave 2, composed of Peak 4 and Trough 4, is downstream from the Plateau (Figure 3). The trends of the wave amplitude at these two spots indicate a flattening signal for Wave 1 and flexing for Wave 2: the meander amplitude in Wave 1 has reduced by 0.31° latitude per decade, indicating that the meander is flattening upstream from the Plateau (Figure 5, Wave 1), while for Wave 2, the meander amplitude has increased by 0.25° latitude per decade, indicating that the meander has been steepening downstream from the Plateau between 1993 and 2020 (Figure 5, Wave 2).

3.3 Observed Changes in Meander Width

Over the 1993-2020 period, the mean width of the meander is 108 km (Figure 4 (b)). Upstream from the Campbell Plateau, the mean width is slightly wider (124 km for the Upstream Section and 117 km for the Plateau Section), while downstream from the Plateau,

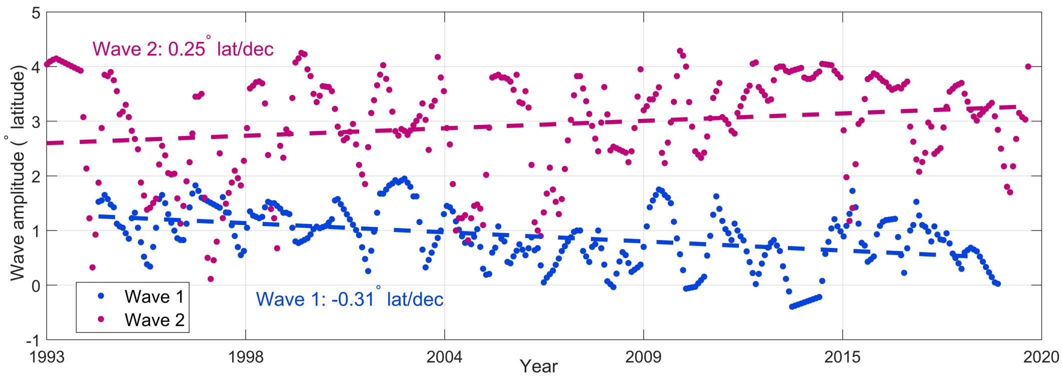

Figure 5. Monthly time series of the Campbell Plateau meander's wave amplitude in degrees latitude (° lat) at Wave 1 (blue dots) and Wave 2 (magenta dots) and corresponding linear trends in degrees latitude per decade (° lat/dec) over the 1993-2020 period (dashed lines).

the mean width is narrower (94 km for the Downstream Section and 85 km for the Flat Region).

Based on our width definition (Figure 2 (b) and (c)), the whole meander has been significantly widening by 2.2 km per decade between 1993 and 2020 (Figure 4 (b); Table 2). Although each section of the meander has a widening trend, the Upstream and Plateau Sections have exhibited a lesser widening as the regions downstream from the Plateau, and their trends are not statistically significant (Figure 4 (b); Table 2). By comparing the widening trend from the Downstream Section (4.2 km per decade) with that from the Flat Region (2.9 km per decade), we find that the Downstream Section contributes most to the overall widening trend (2.2 km per decade) over the 1993-2020 period (Table 2).

3.4 Observed Changes in Meander Speed

Based on the geostrophic current speed estimated from the AVISO data, we find the overall meander has been significantly accelerating by 0.01 m s^{-1} per decade over the 1993-2020 period, which is primarily driven by an acceleration in the Flat Region (Figure 4 (c); Table 2). Similar to the meridional displacement and widening trends, the Upstream and Plateau Sections have almost no change in geostrophic current speed (0.00 m s^{-1} per decade), while the Downstream Section and the Flat Region show an increase in speed (0.02 m s^{-1} per decade) (Figure 4 (c); Table 2). However, only the Flat Region has a significant accelerating trend between 1993 and 2020 (R^2=0.230, p=0.000; Table 2). Shi et al. (2021) report a similar average increase in the surface eastward geostrophic velocity of 0.74±0.25 cm s^{-1} per century (i.e. 0.00074±0.00025 m s^{-1} per decade) between 48°S and 58°S for the entire Southern Ocean over the 1993-2019 period. More interestingly, the various datasets Shi et al. (2021) used (including the AVISO product) identify the area downstream from the Campbell Plateau as a hotspot for this acceleration (Shi et al. (2021), Fig. 5 b). Their estimate of an acceleration of approximately 0.01 m s^{-1} per decade (10 cm s^{-1} per century) matches our estimate of 0.01 m s^{-1} per decade (Figure 4 (c)). Peng et al. (2022) also identify this region as a hotspot for current speed acceleration. Although the overall speed trend is positive and significant, we see that there is large inter-annual and decadal variability in the monthly speed time series (Figure 4 (c)). This variability is beyond the scope of this study but would be worth investigating in future.

4 Discussions and Conclusions

4.1 Position

In this study, we observe that the Upstream and Plateau sections of the meander have not moved significantly in the meridional direction between 1993 and 2020 (Figure 3; Figure 6). This is consistent with previous studies showing no significant meridional displacement of fronts in the Southern Ocean over the past 30 years (e.g., Böning et al. (2008); Graham et al. (2012); Gille (2014); Shao et al. (2015); Freeman et al. (2016); Chapman (2017); Chambers (2018)). This is particularly true in regions near large topographic features, such as the Campbell and Kerguelen Plateaus, which constrain the movement of fronts, leading to the formation of standing meanders. It is noteworthy that absolute value contours, such as dynamic topography contours and sea surface temperature contours have moved southward over similar timescales (Sallée et al., 2008; Sokolov & Rintoul, 2009; Billany et al., 2010; Kim & Orsi, 2014); however, the position of their maximum gradients representing fronts, jets and meanders, has not (Gille, 2014; Chambers, 2018; Chapman et al., 2020). Interestingly, Shao et al. (2015); Freeman et al. (2016) show that the variability in the position of the Polar Front position is strengthened near the Campbell Plateau and the Kerguelen Plateau.

While most of the Campbell Plateau meander (Upstream and Plateau Sections) displays no significant meridional displacement trend, the Downstream Section and, particularly the Flat Region, indicates a significant northward moving trend of about 0.4° latitude per decade (Figure 3; Figure 4 (a); Figure 6). The section upstream from and around the Campbell Plateau is strongly constrained by the local topography, with a low eddy kinetic energy regime (Daniault & Ménard, 1985; Gille et al., 2000; Morrow et al., 2010), making it a true standing meander, however, the section downstream from the Plateau is not constrained by topographic features, and is in a highly dynamical area of the Southern Ocean, with high eddy kinetic energy activity (Gille et al., 2000; Morrow et al., 2010; Y. Zhang et al., 2021; Beech et al., 2022).

We propose two hypotheses to explain the northward displacement of the meander downstream from the Campbell Plateau. Our first hypothesis is that changes in the stability properties of the downstream jet could induce enhanced variability, which in turn leads to a net northward shift of the jet. The meander speed downstream from the Plateau has significantly increased over the 1993-2020 period (Fig 2 (c)), in line with other similar results at larger scales, which, given the minimal changes in width, could result in more shear in the jet, and potentially cause the jet to become more baroclinically unstable (Tansley & Marshall, 2001; Barthel et al., 2017; Youngs et al., 2017; Barthel et al., 2022). Specifically, the zonal jets in this dynamic regime are dominated by baroclinic instability (Youngs et al., 2017; Barthel et al., 2022). Changes in the dynamic stability of the jet could lead to a changing eddy field and, therefore, the ability of the jet to meander downstream, possibly accounting for the observed northward displacement of the Downstream Section. The second hypothesis is that the northward displacement is due to changes in the interaction between the South Pacific Gyre and Antarctic Circumpolar Current jets. The subtropical gyre in the South Pacific Ocean has been accelerating and intensifying since the early 1990s due to the wind stress changes in this area (Cai et al., 2005; Saenko et al., 2005; Qiu & Chen, 2006; Roemmich et al., 2007; C. Liu & Wu, 2012). The South Pacific Gyre is the northern boundary of the Subantarctic Front in the Southern Ocean (Siedler et al., 2013). If the Gyre is contracting and hence the boundary is moving northward, so might the Downstream Section of the meander (Roemmich et al., 2007). While such investigation is beyond the scope of this study, it could be explored through an analysis based on both the realistic and theoretical models (i.e. J. Marshall et al. (1993)).

4.2 Width

We found that the Campbell Plateau meander has been significantly widening by 2.2 km per decade between 1993 and 2020 (Figure 4 (b); Figure 6). It is noteworthy that our definition for the meander width (Figure 2 (b) and (c)) does not consider the individual frontal path, but regards the gradients of absolute dynamic topography as a whole meander. As such, the meander width estimated here might indicate the variability in the meander position over short time scales (about 4 months). When trying to understand the changes in the meander width, we also note that there is very little literature on the width of meanders, fronts and jets in the Southern Ocean. We are aware of two studies, Gille (1994) and Shao et al. (2015), which estimate the width of the Subantarctic Front and the Polar Front over the 1986-1989 and 1992-2013 period, respectively. Gille (1994) shows that the Subantarctic Front and the Polar Front both have a mean width of 44 km (0.4° latitude) in the meridional direction and meander (oscillate around a central point) about 75 km to the northern or southern side of their mean positions. These frontal widths vary by approximately 20% in a broader geographical range (Gille, 1994). Shao et al. (2015) also report similar circumpolar-average widths (85 km) for both the Subantarctic Front and the Polar Front. In the case of the Campbell Plateau meander, its mean width of 108 km between 1993 and 2020 (Figure 4 (b)), while about 2.5 times wider than those in Gille (1994) and 1.3 times wider than those in Shao et al. (2015), it is still comparable, especially considering the differences in the width definitions and existing spatio-temporal viability.

Gille (1994) discusses two factors that impact the width of fronts and jets in the Southern Ocean: baroclinic Rossby radius of deformation R_D, and the conservation of total current transport along the Antarctic Circumpolar Current. The former is also mentioned by Shao et al. (2015) together with another new factor, topography. Gille (1994) and Shao et al. (2015) both demonstrate that the frontal widths estimated in their analysis are correlated with the size of the local value of R_D. This value depends on latitude: narrower when further south and wider when closer to the equator, and on stratification of the water column (Chelton et al., 2011). For the Campbell Plateau meander, its baroclinic Rossby radius is extremely unlikely to have changed over our period of observations. Although the stratification of the water column is changing (Sallée et al., 2021) and the baroclinic Rossby radius is influenced by the stratification, these changes are likely too small to significantly impact the value of the radius (Venaille et al., 2011), and thus cannot explain the widening trend in this study. Shao et al. (2015) also suggest that the narrowing trend of the Polar Front is probably due to changes in the baroclinic Rossby radius (Chelton et al., 2011), which is contrary to the widening trend in our study.

As for topography, Shao et al. (2015) show that the frontal widths will be reduced after passing significant topographic features such as the Campbell Plateau (the width of the Polar Front decreases from 90 km to 50 km while the width of the Subantarctic Front decreases from 100 km to 70 km) and the Kerguelen Plateau (the width of the Polar Front reduces from 90 km to 75 km while the width of the Subantarctic Front reduces from 100 km to 80 km). This matches our observations that the mean width of the Campbell Plateau meander decreases from the Upstream Section to the Downstream Section (from 124 km to 94 km; Figure 4 (b)). These topography-induced narrower frontal widths are possibly caused by the sharpening of jets or the decrease in the distance between jet cores (Shao et al., 2015). Furthermore, in the Downstream Section, where there is almost no topography constraining the flow (Figure 3, Downstream Section), the front may be separated into more jets or become more diffusive (Thompson & Sallée, 2012), which could increase the width of the meander.

Therefore, we are left with changes in the volume transport potentially driving the widening trend of the meander. While there is no detected or modelled trend in the net transport of the Antarctic Circumpolar Current in regions with long observational time-series (Meredith et al., 2011; Koenig et al., 2014; Xu et al., 2020), trends in the individual Southern Ocean front or fronts (e.g., Chouaib et al. (2006)) cannot be ruled out. These trends could potentially contribute to the widening of the Campbell Plateau meander through processes such as enhanced baroclinic instability downstream from the Plateau and increased eddy occurrence (Thompson et al., 2010). Such dynamic adjustments could affect the vertical and horizontal structures in the meander, the latter of which includes its width. Follow-up work regarding the meander width should involve improving the width definition and testing the sensitivity of those previously-derived widening trends to different width definitions. The potential consequences of changes in the meander width would also be worth investigating. For example, the impacts of width changes on cross-frontal transport are relevant across many research fields including the anthropogenic heat and carbon budgets, tracer cycles, upwelling in the Southern Ocean, and even habitat and ecosystem changes (e.g., Hogg et al. (2008); Thompson and Sallée (2012); Barthel et al. (2017); Foppert et al. (2017); Murphy et al. (2021)).

4.3 Geostrophic Current Speed

In this study, we show that the surface geostrophic current speed of the Campbell Plateau meander has been significantly increasing by 0.01 m s^{-1} per decade from 1993 to 2020. This is primarily driven by the acceleration downstream from the Plateau, i.e. the Flat region (0.02 m s^{-1} per decade; Figure 4 (c); Figure 6). These findings are consistent with recent studies investigating the trends in current speed and transport, both globally and in the Southern Ocean (e.g., Roemmich and Gilson (2009); Shi et al. (2021); Peng et al. (2022)).

In the past few decades, the research community has made great efforts to estimate the trends in current speed and understand their driving mechanisms. In the case of the Southern Ocean, the mid-latitude westerly winds are one of the key drivers of the Antarctic Circumpolar Current (Swart & Fyfe, 2012) and they have been observed to intensify from 1950 to the present (Swart & Fyfe, 2012; Fox-Kemper et al., 2021), impacting surface currents. In addition to the westerly winds, however, based on the Community Earth System Model outputs (Gent & Mcwilliams, 1990; Gent & Danabasoglu, 2011), previous studies demonstrate that the buoyancy forcing triggered by ocean warming accelerates the zonal-mean upper-layer (0-2000 m) current in the Southern Ocean more strongly than the wind-driven forcing (Shi et al., 2020). This is due to the fact that the thermal wind response of the zonal current is stronger on the northern edge of the Antarctic Circumpolar Current than within and to the south, leading to higher meridional density gradients (Shi et al., 2020). However, according to the eddy saturation theory (Straub, 1993; Meredith & Hogg, 2006), an increase in the westerly winds over the Southern Ocean would lead to an increase in Ekman transport, which would tilt the isopycnals and cause an increase in the baroclinicity of water masses. This would lead to an increase in eddy kinetic energy, causing the isopycnals to then relax and ultimately, there would be no net wind-induced transport (Hogg & Blundell, 2006; D. Marshall et al., 2017; Meredith & Hogg, 2006). Continuing changes in the wind-driven forcing and ocean warming in the future might even further accelerate the Southern Ocean zonal flow (Fox-Kemper et al., 2021; Shi et al., 2021).

Based on our findings, however, we can not simply attribute the Campbell Plateau meander's overall accelerating trend over the 1993-2020 period to either increased wind forcing or enhanced meridional density gradients. Future work could investigate the meander's eddy kinetic energy trends. By comparing the eddy kinetic energy trends with current speed changes, we could check the role of eddy saturation in the Campbell Plateau Region, which is one of the eddy kinetic energy hotspots in the Southern Ocean (Morrow et al., 2010; Y. Zhang et al., 2021; Beech et al., 2022). It is also worth noting that the increased speed or shear in the front that forms the meander could be either local impacts or global impacts manifesting locally, but it is difficult to disentangle those two mechanisms.

4.4 Changing Meanders in the Southern Ocean

While there are few studies on trends of the Southern Ocean meanders (e.g., Thompson and Naveira Garabato (2014)), our findings for the Campbell Plateau meander can be compared with a recent study on the Agulhas-Kerguelen standing meander by Meyer et al. (2023). They analysed the characteristics and trends of the Agulhas-Kerguelen standing meander over the 1993-2019 period using satellite sea surface height data and similar meander identification methods. Interestingly, the overall trends of both meanders, despite different geographical locations and slightly different dynamical regimes, are similar: no southward migration of the standing meanders and both meanders are widening and accelerating. Observing similar trends in position, wave amplitude, width, and geostrophic current speed for these two meanders suggests that these changes and impacts of these trends on cross-frontal transport of heat, carbon, and other tracers, might not be limited to only one Southern Ocean meander but potentially to many meanders in the Southern Ocean.

4.5 Conclusions

Standing meanders are a special feature of the Southern Ocean, and their response to climate change has been insufficiently studied. In this study, we identified and characterised the Campbell Plateau meander, located south of New Zealand in the Southern Ocean over the 1993-2020 period, using satellite observations. We estimated the position and associated trends in the meander's amplitude, width, and surface geostrophic current speed (see Figure 6 for the summary). Between 1993 and 2020, the position of the Campbell Plateau meander remained relatively stationary, except for a section downstream from the Plateau moving northward by 0.4° latitude per decade. The meander has been flattening at the western edge of the Plateau while flexing at the eastern edge. Moreover, the meander has been significantly widening (2 km per decade) and its surface geostrophic current speed has been increasing (0.01 m s^{-1} per decade), in particular downstream from the Plateau, matching values in the limited existing literature. Interestingly, despite differences in geographical settings and dynamical regimes, the Campbell Plateau meander and the Agulhas-Kerguelen standing meander share similar trends in their position, amplitude, width, and surface geostrophic current speed. Future work should investigate the drivers behind the changes in the Campbell Plateau meander's amplitude and resulting dynamic adjustments, along with the impacts of these observed trends on the cross-frontal transport of the Antarctic Circumpolar Current.

5 Data Availability Statement

The satellite altimetry absolute dynamic topography data as well as zonal and meridional surface geostrophic current velocities data (Product: Global Ocean Gridded L 4 Sea Surface Heights And Derived Variables Reprocessed 1993 Ongoing) used for identifying, characterising and analysing the trends of the Campbell Plateau meander in the study are publicly available at Marine Data Store, European Union Copernicus Marine Environment Monitoring Service via `https://doi.org/10.48670/moi-00148` (CMEMS, 2019). The bathymetric data used for mapping the local bathymetry in the Campbell Plateau region in the study are publicly available at Global Multi-Resolution Topography GridServer Web Service via `https://www.gmrt.org/services/gridserverinfo.php#!/services/getGMRTGrid` (Ryan et al., 2009). MATLAB R2020a was used for analysing the characteristics and trends of the Campbell Plateau meander. The MATLAB cmocean perceptually-uniform colourmaps toolbox used for plotting the colourmaps of Figure 1 and Figure 2 in the study are publicly available at GitHub via `https://github.com/chadagreene/cmocean` (Thyng et al., 2016).

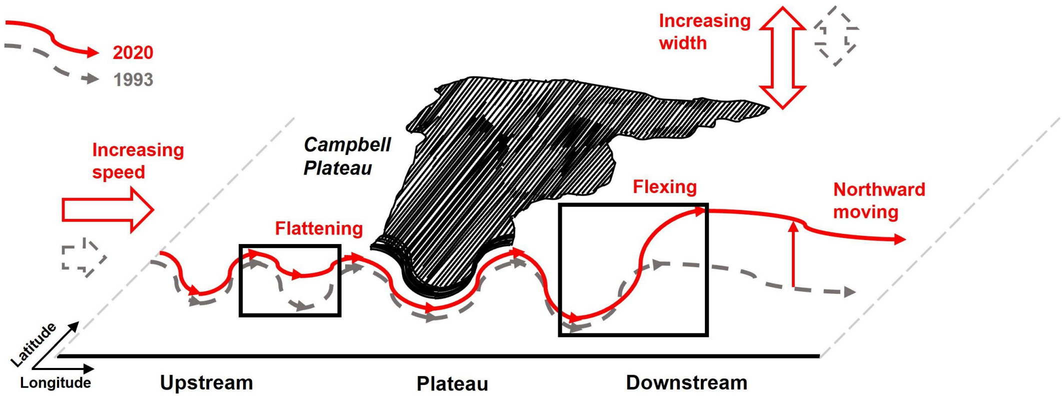

Figure 6. Schematic illustrating the trends of the Campbell Plateau meander's position, flattening and flexing of the meander's shape, widening of the meander in some parts, and increasing geostrophic current speed over the 1993-2020 period. The Campbell Plateau is represented by the shaded area. This schematic is based on and modified from FIG. 16 in X. Zhang et al. (2022).

Acknowledgments

We are thankful for the collaboration between the University of Tasmania and the Ocean University of China (K4C 2+2 Honours Program) that provided support to conduct this research. XL acknowledges support from the Overseas Learning Centre at the Ocean University of China and from the Australian Research Council Centre of Excellence for Climate Extremes and the Institute for Marine and Antarctic Studies for his Honours year. XL and AM are supported by the Australian Research Council (ARC) Centre of Excellence of Climate Extremes (CLEX; ARC Grant No. CE170100023). CC acknowledges financial support from the Centre for Southern Hemisphere Ocean Research (CSHOR). We thank two anonymous assessors from the Institute for Marine and Antarctic Studies for their feedback on this work. We also thank Xihan Zhang and Stuart Corney from the Institute for Marine and Antarctic Studies for their comments on this paper. Open access publishing facilitated by the University of Tasmania, as part of the Wiley-University of Tasmania agreement via the Council of Australian University Librarians.

References

Bachman, S. D., Taylor, J., Adams, K., & Hosegood, P. (2017). Mesoscale and submesoscale effects on mixed layer depth in the southern ocean. *Journal of Physical Oceanography*, *47*(9), 2173–2188.

Barthel, A., Hogg, A. M., Waterman, S., & Keating, S. (2022). Baroclinic control of southern ocean eddy upwelling near topography. *Geophysical Research Letters*, e2021GL097491.

Barthel, A., McC. Hogg, A., Waterman, S., & Keating, S. (2017). Jet–topography interactions affect energy pathways to the deep southern ocean. *Journal of Physical Oceanography*, *47*(7), 1799–1816.

Beech, N., Rackow, T., Semmler, T., Danilov, S., Wang, Q., & Jung, T. (2022). Long-term evolution of ocean eddy activity in a warming world. *Nature climate change*, *12*(10), 910–917.

Billany, W., Swart, S., Hermes, J., & Reason, C. (2010). Variability of the southern ocean fronts at the greenwich meridian. *Journal of Marine Systems*, *82*(4), 304–310.

Bindoff, N. L., Cheung, W. W., Kairo, J. G., Arístegui, J., Guinder, V. A., Hallberg, R., . . . Williamson, P. (2019). Changing ocean, marine ecosystems, and dependent communities. In H.-O. Pörtner et al. (Eds.), *Ipcc special report on the ocean and cryosphere in a changing climate* (pp. 447–587). Cambridge, UK and New York, NY, USA: Cambridge University Press. Retrieved from https://doi.org/10.1017\%2F9781009157964.007 doi: 10.1017/9781009157964.007

Böning, C. W., Dispert, A., Visbeck, M., Rintoul, S., & Schwarzkopf, F. U. (2008). The response of the antarctic circumpolar current to recent climate change. *Nature Geoscience*, *1*(12), 864–869.

Brady, R. X., Maltrud, M. E., Wolfram, P. J., Drake, H. F., & Lovenduski, N. S. (2021). The influence of ocean topography on the upwelling of carbon in the southern ocean. *Geophysical Research Letters*, *48*(19), e2021GL095088.

Cai, W., Shi, G., Cowan, T., Bi, D., & Ribbe, J. (2005). The response of the southern annular mode, the east australian current, and the southern mid-latitude ocean circulation to global warming. *Geophysical Research Letters*, *32*(23).

Carter, L., & Wilkin, J. (1999). Abyssal circulation around new zealand—a comparison between observations and a global circulation model. *Marine Geology*, *159*(1-4), 221–239.

Chambers, D. P. (2018). Using kinetic energy measurements from altimetry to detect shifts in the positions of fronts in the southern ocean. *Ocean Science*, *14*(1), 105–116.

Chapman, C. C. (2014). Southern ocean jets and how to find them: Improving and comparing common jet detection methods. *Journal of Geophysical Research: Oceans*, *119*(7), 4318–4339.

Chapman, C. C. (2017). New perspectives on frontal variability in the southern ocean. *Journal of Physical Oceanography*, *47*(5), 1151–1168.

Chapman, C. C., Hogg, A. M., Kiss, A. E., & Rintoul, S. R. (2015). The dynamics of southern ocean storm tracks. *Journal of Physical Oceanography*, *45*(3), 884–903.

Chapman, C. C., Lea, M.-A., Meyer, A., Sallée, J.-B., & Hindell, M. (2020). Defining southern ocean fronts and their influence on biological and physical processes in a changing climate. *Nature Climate Change*, *10*(3), 209–219.

Chapman, C. C., & Morrow, R. (2014). Variability of southern ocean jets near topography. *Journal of physical oceanography*, *44*(2), 676–693.

Chapman, C. C., & Sallée, J.-B. (2017). Isopycnal mixing suppression by the antarctic circumpolar current and the southern ocean meridional overturning circulation. *Journal of Physical Oceanography*, *47*(8), 2023–2045.

Chelton, D. B., Schlax, M. G., & Samelson, R. M. (2011). Global observations of nonlinear mesoscale eddies. *Progress in oceanography*, *91*(2), 167–216.

Chouaib, N., Stoehr, F., & Provost, C. (2006). Variability of the subantarctic and polar fronts in the drake passage as deduced from altimetry. *Journal of marine research*, *64*(5), 669–693.

CMEMS. (2019). *Global ocean gridded l4 sea surface heights and derived variables reprocessed (1993-ongoing)* [dataset]. Copernicus Marine Environment Monitoring Service. Retrieved from https://data.marine.copernicus.eu/product/SEALEVEL_GLO_PHY_L4_MY_008_047 doi: 10.48670/moi-00148

Cyriac, A., Meyer, A., Phillips, H., & Bindoff, N. (2023). Observations of internal wave interactions in a southern ocean standing meander. *Journal of Physical Oceanography*, under review.

Daniault, N., & Ménard, Y. (1985). Eddy kinetic energy distribution in the southern ocean from altimetry and fgge drifting buoys. *Journal of Geophysical Research: Oceans*, *90*(C6), 11877–11889.

Deacon, G. E. R. (1937). The hydrology of the southern ocean. *Discovery Rep.*, *15*, 3–122.

Dong, S., Sprintall, J., & Gille, S. T. (2006). Location of the antarctic polar front from amsr-e satellite sea surface temperature measurements. *Journal of Physi-*

cal Oceanography, *36*(11), 2075–2089.
Donohue, K., Tracey, K., Watts, D., Chidichimo, M. P., & Chereskin, T. (2016). Mean antarctic circumpolar current transport measured in drake passage. *Geophysical Research Letters*, *43*(22), 11–760.
Dove, L. A., Balwada, D., Thompson, A. F., & Gray, A. R. (2022). Enhanced ventilation in energetic regions of the antarctic circumpolar current. *Geophysical Research Letters*, *49*(13), e2021GL097574.
Dove, L. A., Thompson, A. F., Balwada, D., & Gray, A. R. (2021). Observational evidence of ventilation hotspots in the southern ocean. *Journal of Geophysical Research: Oceans*, *126*(7), e2021JC017178.
Foppert, A., Donohue, K. A., Watts, D. R., & Tracey, K. L. (2017). Eddy heat flux across the antarctic circumpolar current estimated from sea surface height standard deviation. *Journal of Geophysical Research: Oceans*, *122*(8), 6947–6964.
Forcén-Vázquez, A., Williams, M. J., Bowen, M., Carter, L., & Bostock, H. (2021). Frontal dynamics and water mass variability on the campbell plateau. *New Zealand Journal of Marine and Freshwater Research*, *55*(1), 199–222.
Fox-Kemper, B., Hewitt, H. T., Xiao, C., Aoalgeirsdóttir, G., Drijfhout, S. S., Edwards, T. L., … Yu, Y. (2021). Ocean, cryosphere and sea level change [Book Section]. In V. Masson-Delmotte et al. (Eds.), *Climate change 2021: The physical science basis. contribution of working group i to the sixth assessment report of the intergovernmental panel on climate change* (chap. 9). Cambridge, United Kingdom and New York, NY, USA: Cambridge University Press. Retrieved from https://www.ipcc.ch/report/ar6/wg1/downloads/report/IPCC_AR6_WGI_Chapter_09.pdf
Freeman, N. M., Lovenduski, N. S., & Gent, P. R. (2016). Temporal variability in the antarctic polar front (2002–2014). *Journal of Geophysical Research: Oceans*, *121*(10), 7263–7276.
Frölicher, T. L., Sarmiento, J. L., Paynter, D. J., Dunne, J. P., Krasting, J. P., & Winton, M. (2015). Dominance of the southern ocean in anthropogenic carbon and heat uptake in cmip5 models. *Journal of Climate*, *28*(2), 862–886.
Gent, P. R., & Danabasoglu, G. (2011). Response to increasing southern hemisphere winds in ccsm4. *Journal of climate*, *24*(19), 4992–4998.
Gent, P. R., & Mcwilliams, J. C. (1990). Isopycnal mixing in ocean circulation models. *Journal of Physical Oceanography*, *20*(1), 150–155.
Gille, S. T. (1994). Mean sea surface height of the antarctic circumpolar current from geosat data: Method and application. *Journal of Geophysical Research: Oceans*, *99*(C9), 18255–18273.
Gille, S. T. (2014). Meridional displacement of the antarctic circumpolar current. *Philosophical Transactions of the Royal Society A: Mathematical, Physical and Engineering Sciences*, *372*(2019), 20130273.
Gille, S. T., & Kelly, K. A. (1996). Scales of spatial and temporal variability in the southern ocean. *Journal of Geophysical Research: Oceans*, *101*(C4), 8759–8773.
Gille, S. T., Yale, M. M., & Sandwell, D. T. (2000). Global correlation of mesoscale ocean variability with seafloor roughness from satellite altimetry. *Geophysical Research Letters*, *27*(9), 1251–1254.
Gordon, A. (1972). The australian-new zealand sector. *Antarct. Res. Ser.*, *19*.
Graham, R. M., De Boer, A. M., Heywood, K. J., Chapman, M. R., & Stevens, D. P. (2012). Southern ocean fronts: Controlled by wind or topography? *Journal of Geophysical Research: Oceans*, *117*(C8).
Heath, R. (1981). Oceanic fronts around southern new zealand. *Deep Sea Research Part A. Oceanographic Research Papers*, *28*(6), 547–560.
Hogg, A. M. C., & Blundell, J. R. (2006). Interdecadal variability of the southern ocean. *Journal of physical oceanography*, *36*(8), 1626–1645.

Hogg, A. M. C., Meredith, M. P., Blundell, J. R., & Wilson, C. (2008). Eddy heat flux in the southern ocean: Response to variable wind forcing. *Journal of Climate*, *21*(4), 608–620.
Hughes, C. W. (2005). Nonlinear vorticity balance of the antarctic circumpolar current. *Journal of Geophysical Research: Oceans*, *110*(C11).
Hughes, C. W., & Ash, E. R. (2001). Eddy forcing of the mean flow in the southern ocean. *Journal of Geophysical Research: Oceans*, *106*(C2), 2713–2722.
Killworth, P. D. (1992). An equivalent-barotropic mode in the fine resolution antarctic model. *Journal of Physical Oceanography*, *22*(11), 1379–1387.
Kim, Y. S., & Orsi, A. H. (2014). On the variability of antarctic circumpolar current fronts inferred from 1992–2011 altimetry. *Journal of Physical Oceanography*, *44*(12), 3054–3071.
Klocker, A. (2018). Opening the window to the southern ocean: The role of jet dynamics. *Science advances*, *4*(10), eaao4719.
Koenig, Z., Provost, C., Ferrari, R., Sennéchael, N., & Rio, M.-H. (2014). Volume transport of the a ntarctic c ircumpolar c urrent: Production and validation of a 20 year long time series obtained from in situ and satellite observations. *Journal of Geophysical Research: Oceans*, *119*(8), 5407–5433.
Langlais, C., Lenton, A., Matear, R., Monselesan, D., Legresy, B., Cougnon, E., & Rintoul, S. (2017). Stationary rossby waves dominate subduction of anthropogenic carbon in the southern ocean. *Scientific reports*, *7*(1), 1–10.
Langlais, C., Rintoul, S., & Schiller, A. (2011). Variability and mesoscale activity of the southern ocean fronts: Identification of a circumpolar coordinate system. *Ocean Modelling*, *39*(1-2), 79–96.
Liu, C., & Wu, L. (2012). An intensification trend of south pacific mode water subduction rates over the 20th century. *Journal of Geophysical Research: Oceans*, *117*(C7).
Liu, X. (2022). *Characteristics and trends of the campbell plateau meander in the southern ocean* (Honours thesis, University of Tasmania). doi: 10.25959/100.00047676
Llort, J., Langlais, C., Matear, R., Moreau, S., Lenton, A., & Strutton, P. G. (2018). Evaluating southern ocean carbon eddy-pump from biogeochemical-argo floats. *Journal of Geophysical Research: Oceans*, *123*(2), 971–984.
Lu, J., & Speer, K. (2010). Topography, jets, and eddy mixing in the southern ocean. *Journal of Marine Research*, *68*(3-4), 479–502.
Lumpkin, R., & Speer, K. (2007). Global ocean meridional overturning. *Journal of Physical Oceanography*, *37*(10), 2550–2562.
Marshall, D., Ambaum, M. H., Maddison, J. R., Munday, D. R., & Novak, L. (2017). Eddy saturation and frictional control of the antarctic circumpolar current. *Geophysical research letters*, *44*(1), 286–292.
Marshall, J., Olbers, D., Ross, H., & Wolf-Gladrow, D. (1993). Potential vorticity constraints on the dynamics and hydrography of the southern ocean. *Journal of Physical Oceanography*, *23*(3), 465–487.
Marshall, J., & Speer, K. (2012). Closure of the meridional overturning circulation through southern ocean upwelling. *Nature geoscience*, *5*(3), 171–180.
McDougall, T. J., & Klocker, A. (2010). An approximate geostrophic streamfunction for use in density surfaces. *Ocean Modelling*, *32*(3-4), 105–117.
Meijer, J. J., Phillips, H. E., Bindoff, N. L., Rintoul, S. R., & Foppert, A. (2022). Dynamics of a standing meander of the subantarctic front diagnosed from satellite altimetry and along-stream anomalies of temperature and salinity. *Journal of Physical Oceanography*, *52*(6), 1073–1089.
Meredith, M. P., & Hogg, A. M. (2006). Circumpolar response of southern ocean eddy activity to a change in the southern annular mode. *Geophysical Research Letters*, *33*(16).
Meredith, M. P., Woodworth, P. L., Chereskin, T. K., Marshall, D. P., Allison,

L. C., Bigg, G. R., ... others (2011). Sustained monitoring of the southern ocean at drake passage: Past achievements and future priorities. *Reviews of Geophysics*, *49*(4).

Meyer, A., Langlais, C., Constantinou, N., Legresy, N., McC. Hogg, A., Navid, C., & Bindoff, N. (2023). Southern ocean meander structure trends and implications for carbon and heat uptake under a changing climate. *personal communication*.

Mikaloff Fletcher, S. E., Gruber, N., Jacobson, A. R., Doney, S. C., Dutkiewicz, S., Gerber, M., ... others (2006). Inverse estimates of anthropogenic co2 uptake, transport, and storage by the ocean. *Global biogeochemical cycles*, *20*(2).

Moore, J. K., Abbott, M. R., & Richman, J. G. (1997). Variability in the location of the antarctic polar front (90–20 w) from satellite sea surface temperature data. *Journal of Geophysical Research: Oceans*, *102*(C13), 27825–27833.

Moore, J. K., Abbott, M. R., & Richman, J. G. (1999). Location and dynamics of the antarctic polar front from satellite sea surface temperature data. *Journal of Geophysical Research: Oceans*, *104*(C2), 3059–3073.

Morris, M., Stanton, B., & Neil, H. (2001). Subantarctic oceanography around new zealand: preliminary results from an ongoing survey. *New Zealand Journal of Marine and Freshwater Research*, *35*(3), 499–519.

Morrison, A. K., Frölicher, T. L., & Sarmiento, J. L. (2015). Upwelling in the southern ocean. *Physics Today*, *68*(1), 27.

Morrow, R., Ward, M. L., Hogg, A. M., & Pasquet, S. (2010). Eddy response to southern ocean climate modes. *Journal of Geophysical Research: Oceans*, *115*(C10).

Murphy, E. J., Johnston, N. M., Hofmann, E. E., Phillips, R. A., Jackson, J. A., Constable, A. J., ... others (2021). Global connectivity of southern ocean ecosystems. *Frontiers in Ecology and Evolution*, 454.

Nardelli, B. B. (2013). Vortex waves and vertical motion in a mesoscale cyclonic eddy. *Journal of Geophysical Research: Oceans*, *118*(10), 5609–5624.

Naveira Garabato, A. C., Ferrari, R., & Polzin, K. L. (2011). Eddy stirring in the southern ocean. *Journal of Geophysical Research: Oceans*, *116*(C9).

Neil, H. L., Carter, L., & Morris, M. Y. (2004). Thermal isolation of campbell plateau, new zealand, by the antarctic circumpolar current over the past 130 kyr. *Paleoceanography*, *19*(4).

Newton, C. W. (1959). *Synoptic comparisons of jet stream and gulf stream systems* (Tech. Rep.). Chicago, Illinois, United States: University of Illinois Chicago.

Olbers, D., Borowski, D., Völker, C., & WOeLFF, J.-O. (2004). The dynamical balance, transport and circulation of the antarctic circumpolar current. *Antarctic science*, *16*(4), 439–470.

Orsi, A. H., Whitworth III, T., & Nowlin Jr, W. D. (1995). On the meridional extent and fronts of the antarctic circumpolar current. *Deep Sea Research Part I: Oceanographic Research Papers*, *42*(5), 641–673.

Peng, Q., Xie, S.-P., Wang, D., Huang, R. X., Chen, G., Shu, Y., ... Liu, W. (2022). Surface warming–induced global acceleration of upper ocean currents. *Science Advances*, *8*(16), eabj8394.

Phillips, H., & Bindoff, N. (2014). On the nonequivalent barotropic structure of the antarctic circumpolar current: An observational perspective. *Journal of Geophysical Research: Oceans*, *119*(8), 5221–5243.

Qiu, B., & Chen, S. (2006). Decadal variability in the large-scale sea surface height field of the south pacific ocean: Observations and causes. *Journal of physical oceanography*, *36*(9), 1751–1762.

Rintoul, S., & Naveira Garabato, A. (2013). Dynamics of the southern ocean circulation. In *International geophysics* (Vol. 103, pp. 471–492). Elsevier.

Rintoul, S., Sokolov, S., Williams, M., Peña Molino, B., Rosenberg, M., & Bindoff, N. (2014). Antarctic circumpolar current transport and barotropic transition at macquarie ridge. *Geophysical Research Letters*, *41*(20), 7254–7261.

Roach, C. J., Balwada, D., & Speer, K. (2016). Horizontal mixing in the southern ocean from argo float trajectories. *Journal of Geophysical Research: Oceans*, *121*(8), 5570–5586.

Roemmich, D., & Gilson, J. (2009). The 2004–2008 mean and annual cycle of temperature, salinity, and steric height in the global ocean from the argo program. *Progress in oceanography*, *82*(2), 81–100.

Roemmich, D., Gilson, J., Davis, R., Sutton, P., Wijffels, S., & Riser, S. (2007). Decadal spinup of the south pacific subtropical gyre. *Journal of Physical Oceanography*, *37*(2), 162–173.

Rosso, I., Hogg, A. M., Kiss, A. E., & Gayen, B. (2015). Topographic influence on submesoscale dynamics in the southern ocean. *Geophysical Research Letters*, *42*(4), 1139–1147.

Ryan, W. B., Carbotte, S. M., Coplan, J. O., O'Hara, S., Melkonian, A., Arko, R., ... others (2009). Global multi-resolution topography synthesis. *Geochemistry, Geophysics, Geosystems*, *10*(3).

Sabine, C. L., Feely, R. A., Gruber, N., Key, R. M., Lee, K., Bullister, J. L., ... others (2004). The oceanic sink for anthropogenic co2. *science*, *305*(5682), 367–371.

Saenko, O. A., Fyfe, J. C., & England, M. H. (2005). On the response of the oceanic wind-driven circulation to atmospheric co2 increase. *Climate dynamics*, *25*, 415–426.

Sallée, J.-B., Matear, R. J., Rintoul, S. R., & Lenton, A. (2012). Localized subduction of anthropogenic carbon dioxide in the southern hemisphere oceans. *Nature Geoscience*, *5*(8), 579–584.

Sallée, J.-B., Pellichero, V., Akhoudas, C., Pauthenet, E., Vignes, L., Schmidtko, S., ... Kuusela, M. (2021). Summertime increases in upper-ocean stratification and mixed-layer depth. *Nature*, *591*(7851), 592–598.

Sallée, J.-B., Speer, K., & Morrow, R. (2008). Response of the antarctic circumpolar current to atmospheric variability. *Journal of Climate*, *21*(12), 3020–3039.

Sarmiento, J. L., Gruber, N., Brzezinski, M., & Dunne, J. (2004). High-latitude controls of thermocline nutrients and low latitude biological productivity. *Nature*, *427*(6969), 56–60.

Shao, A. E., Gille, S. T., Mecking, S., & Thompson, L. (2015). Properties of the subantarctic front and polar front from the skewness of sea level anomaly. *Journal of Geophysical Research: Oceans*, *120*(7), 5179–5193.

Shi, J.-R., Talley, L. D., Xie, S.-P., Liu, W., & Gille, S. T. (2020). Effects of buoyancy and wind forcing on southern ocean climate change. *Journal of Climate*, *33*(23), 10003–10020.

Shi, J.-R., Talley, L. D., Xie, S.-P., Peng, Q., & Liu, W. (2021). Ocean warming and accelerating southern ocean zonal flow. *Nature Climate Change*, *11*(12), 1090–1097.

Siedler, G., Griffies, S., Gould, J., & Church, J. (2013). *Ocean circulation and climate: a 21st century perspective*. Academic Press.

Sokolov, S., & Rintoul, S. R. (2002). Structure of southern ocean fronts at 140 e. *Journal of Marine Systems*, *37*(1-3), 151–184.

Sokolov, S., & Rintoul, S. R. (2007a). Multiple jets of the antarctic circumpolar current south of australia. *Journal of Physical Oceanography*, *37*(5), 1394–1412.

Sokolov, S., & Rintoul, S. R. (2007b). On the relationship between fronts of the antarctic circumpolar current and surface chlorophyll concentrations in the southern ocean. *Journal of Geophysical Research: Oceans*, *112*(C7).

Sokolov, S., & Rintoul, S. R. (2009). Circumpolar structure and distribution of the antarctic circumpolar current fronts: 2. variability and relationship to sea surface height. *Journal of Geophysical Research: Oceans*, *114*(C11).

Straub, D. N. (1993). On the transport and angular momentum balance of channel models of the antarctic circumpolar current. *Journal of physical oceanography*, *23*(4), 776–782.

Swart, N., & Fyfe, J. C. (2012). Observed and simulated changes in the southern hemisphere surface westerly wind-stress. *Geophysical Research Letters*, *39*(16).

Tamsitt, V., Drake, H. F., Morrison, A. K., Talley, L. D., Dufour, C. O., Gray, A. R., ... others (2017). Spiraling pathways of global deep waters to the surface of the southern ocean. *Nature communications*, *8*(1), 172.

Tansley, C. E., & Marshall, D. P. (2001). Flow past a cylinder on a β plane, with application to gulf stream separation and the antarctic circumpolar current. *Journal of Physical Oceanography*, *31*(11), 3274–3283.

Thomas, S. D., Jones, D. C., Faul, A., Mackie, E., & Pauthenet, E. (2021). Defining southern ocean fronts using unsupervised classification. *Ocean Science*, *17*(6), 1545–1562.

Thompson, A. F. (2010). Jet formation and evolution in baroclinic turbulence with simple topography. *Journal of Physical Oceanography*, *40*(2), 257–278.

Thompson, A. F., Haynes, P. H., Wilson, C., & Richards, K. J. (2010). Rapid southern ocean front transitions in an eddy-resolving ocean gcm. *Geophysical research letters*, *37*(23).

Thompson, A. F., & Naveira Garabato, A. C. (2014). Equilibration of the antarctic circumpolar current by standing meanders. *Journal of Physical Oceanography*, *44*(7), 1811–1828.

Thompson, A. F., & Sallée, J.-B. (2012). Jets and topography: Jet transitions and the impact on transport in the antarctic circumpolar current. *Journal of physical Oceanography*, *42*(6), 956–972.

Thyng, K. M., Greene, C. A., Hetland, R. D., Zimmerle, H. M., & DiMarco, S. F. (2016). True colors of oceanography: Guidelines for effective and accurate colormap selection. *Oceanography*, *29*(3), 9–13.

Toggweiler, J., & Samuels, B. (1995). Effect of drake passage on the global thermohaline circulation. *Deep Sea Research Part I: Oceanographic Research Papers*, *42*(4), 477–500.

Venaille, A., Vallis, G. K., & Smith, K. S. (2011). Baroclinic turbulence in the ocean: Analysis with primitive equation and quasigeostrophic simulations. *Journal of Physical Oceanography*, *41*(9), 1605–1623.

Viglione, G. A., & Thompson, A. F. (2016). Lagrangian pathways of upwelling in the southern ocean. *Journal of Geophysical Research: Oceans*, *121*(8), 6295–6309.

Witter, D. L., & Chelton, D. B. (1998). Eddy–mean flow interaction in zonal oceanic jet flow along zonal ridge topography. *Journal of physical oceanography*, *28*(10), 2019–2039.

Xu, X., Chassignet, E. P., Firing, Y. L., & Donohue, K. (2020). Antarctic circumpolar current transport through drake passage: what can we learn from comparing high-resolution model results to observations? *Journal of Geophysical Research: Oceans*, *125*(7), e2020JC016365.

Youngs, M. K., Thompson, A. F., Lazar, A., & Richards, K. J. (2017). Acc meanders, energy transfer, and mixed barotropic–baroclinic instability. *Journal of Physical Oceanography*, *47*(6), 1291–1305.

Zhang, X., Nikurashin, M., Peña-Molino, B., Rintoul, S. R., & Doddridge, E. (2022). A theory of standing meanders of the antarctic circumpolar current and their response to wind. *Journal of Physical Oceanography*.

Zhang, Y., Chambers, D., & Liang, X. (2021). Regional trends in southern ocean eddy kinetic energy. *Journal of Geophysical Research: Oceans*, *126*(6), e2020JC016973.